INTERNATIONAL JOURNAL OF AUTOMOTIVE AND MECHANICAL ENGINEERING
ISSN: 2229-8649 e-ISSN: 2180-1606
VOLUME 22, ISSUE 4, 2025, 13002 - 13018
DOI: https://doi.org/10.15282/ijame.22.4.2025.12.0989

RESEARCH ARTICLE

Cooling Slope-Cast LM25 Aluminum Fabrication for Additive Friction Stir Deposition: A Microstructural and Mechanical Study

S. C. Tham[1], M. K. Sued[1]*, M. S. Salleh[1], N. I. S. Hussein[1], R. Muslim[2], A. S. Anuar[1], M. M. Abdulatef[1]

[1]Fakulti Teknologi dan Kejuruteraan Industri dan Pembuatan, Universiti Teknikal Malaysia Melaka, Hang Tuah Jaya, 76100 Durian Tunggal, Melaka, Malaysia

[2]Mechanical Engineering of Vocational School, Universitas Sebelas Maret, 57126, Indonesia

ABSTRACT – Additive Friction Stir Deposition (AFSD) is an innovative solid-state additive manufacturing (AM) technique that has offered a promising solution for joining and fabricating high-performance aluminum alloys over the past decade. However, the use of heat-treated feedstock produced by cooling slope casting (CSC) remains largely unexplored. This initial study investigates the feasibility of using CSC LM25 feedstock in AFSD to achieve better microstructure and hardness, while preventing early feedstock breakage. Microstructural examination indicated a shift from coarse dendritic to globular grains, with an average grain size of 1.828 µm (0.351-60.835 µm), a reduction of approximately 96.3% compared to the as-cast material. While some samples (notably C5 CSC_HT and D2 PMC_HT) achieved smooth, defect-free deposition, continuous deposits under higher rotational speed (800 rpm) and feed rate (3 mm/min), the hardness of deposited parts reduced to 63–72 HV compared to 89HV in the base material, reflecting a ~20–29% decline due to thermal softening, over-aging of precipitates, and Si coarsening during AFSD thermal cycles. Although CSC helped to refine the grain structure and enhance deposition flow, this alone was not enough to improve the mechanical behavior of the deposited parts. Additional processing steps, such as thixoforming or heat treatment after deposition, may be needed to achieve better results. This study offers early observations on how cast feedstock behaves in AFSD and identifies important challenges and future directions for improving the solid-state processing of aluminum alloys, especially for lightweight parts in aerospace and automotive applications.

ARTICLE HISTORY
Received : 10th July 2025
Revised : 12th Sept. 2025
Accepted : 22nd Oct. 2025
Published : 16th Nov. 2025

KEYWORDS
Additive friction stir deposition (AFSD)
Cooling slope casting,
Aluminum alloy feedstock,
T6 heat treatment,
Solid-state additive manufacturing

1. INTRODUCTION

LM25 aluminum alloy, also known as A356 or AlSi7Mg, is a popular casting alloy renowned for its excellent castability, mechanical properties, and corrosion resistance. Its outstanding strength-to-weight ratio makes it perfect for automotive, aeronautical, and other engineering applications needing lightweight yet robust components [1], [2] Recent Surani (2024) and Sunitha (2022) studies show that LM25 appears to enhance the metallurgical characteristics of aluminum cast alloys under heat treatments while also exhibiting better mechanical performance [3], [4]; wrought aluminum alloys, such as wrought 6061 and 7075 aluminum alloys, seem to provide the same outcomes under heat treatments [5], [6], [7]. The ultimate tensile strength, for example, can exceed 210 MPa for Thixoformed-T6 A356 alloy [8] and more than 250 MPa for Thixoformed-T6 (Solution Treatment-30 min) LM4 alloy [9], making these cast aluminum alloys a strong candidate for load-bearing applications. Recent studies also demonstrate that cast alloys processed via Additive Friction Stir Deposition (AFSD) can undergo significant microstructural refinement and strengthening compared to their as-cast state, as observed in high-entropy alloys [10]. These findings highlight the broader potential of extending AFSD to LM25 as a high-performance cast alloy.

While LM25 is well-studied in casting and heat treatment, there is limited research on its use in additive friction stir deposition (AFSD), especially when using cast aluminum feedstock. Most AFSD processes to date have used extruded or bar-shaped aluminum rods as feedstock, largely because they are readily available and easy to handle during deposition [11]. However, these rods typically have a fixed microstructure which, combined with the need for standard-sized feed rods to suit specific AFSD machine designs, limits opportunities for metallurgical modification during deposition [12]. Although it is technically possible to use both cast and wrought forms as AFSD feed materials, the selection, preparation, and performance of cast feedstock remain underexplored areas, particularly in terms of deposition reliability and structural integrity [12]. Studies have reported typical issues such as porosity, weak bonding, flash formation, and local melting when using cast feedstock, all of which compromise final part quality [13]. These problems are even more severe when AFSD is performed using FSW machines, where the parameters are not originally designed for additive processes. Researchers have pointed out that adapting existing FSW equipment for AFSD can be difficult due to limitations in flexibility, control, and material compatibility [12]. This has also been seen in recent experiments with high-temperature materials, where the machine hardware struggled to handle the thermal and mechanical demands of the process [14]. For example, Alzahrani et al. (2021) found that even small changes in feed rate or speed significantly impacted defect

***CORRESPONDING AUTHOR | Mohammad Kamil Sued** | ✉ kamil@utem.edu.my

formation in cast A356 during AFSD, while Dilip et al. (2013) highlighted the need for precise parameter control to achieve sound bonding in multilayer aluminum deposits in AA2014 alloys [15], [16]. Furthermore, Soni (2025) reported exceptional as-deposited strength, ductility synergy in Al–Ce alloys processed via AFSD, demonstrating the solid-state process's ability to overcome fusion-related defects and refine microstructures [17]. These findings reinforce the need for alternative feedstock strategies and process optimization, thereby motivating the present study on cooling slope cast LM25 as a reliable input for AFSD.

CSC has been shown to refine grain structure and improve material flow, making it a promising alternative to extruded feed rods. Previous studies on A356, A319, and LM4 alloys confirm that CSC effectively transforms coarse dendritic structures into fine, globular morphologies, thereby enhancing feedstock consistency and improving mechanical properties [18], [19], [20]. Thus, while extruded rods have dominated AFSD research due to their availability, their fixed microstructure limits metallurgical flexibility and constrains performance improvements. This reinforces the need to test alternative feedstocks such as CSC-derived LM25. While LM25 has been extensively studied under casting and heat-treatment conditions, its use as CSC feedstock in AFSD has not been reported. To the best of the researcher's knowledge, no prior study has combined CSC with AFSD for LM25 aluminum alloy, and this is still underexplored. Hence, the main objective of this study is to develop and evaluate a cooling-slope cast LM25 feedstock for use in additive friction stir deposition (AFSD) and to compare its microstructural and mechanical properties with those of conventionally cast material. It should be noted that this work is an early pilot study, limited to single-layer deposition and does not include tensile or wear testing; such investigations, along with multilayer builds, are planned as future work. This research is intended to generate practical insights for industrial applications, especially in areas where high-strength, lightweight materials are essential. More than just a technical enhancement, the study seeks to contribute to best practices in advanced manufacturing, addressing the growing demands of modern engineering challenges.

1.1 Cooling Slope Casting Technique

Employing a novel technique called cooling slope casting in semi-solid processing enables metal-controlled solidification, thereby improving the mechanical characteristics of cast alloys. As illustrated in Figure 1, molten metal is poured from the crucible onto an inclined cooling slope, typically positioned between 30° and 60°. As the melt flows downward, temperature gradients and fluid motion generate shear forces that initiate the nucleation and breakup of primary dendrites. This process converts the liquid metal into a semi-solid slurry with a globular microstructure [18], [19], [20]. The slurry subsequently enters a water-cooled mold, where it solidifies to form castings with refined, non-dendritic grains and superior mechanical properties compared to those of as-cast final products. Common problems in the conventional casting techniques, such as reduced segregation and porosity, are among the advantages of this process [19], [21], [22]. Research has demonstrated that cooling slope casting can effectively minimize shrinkage and porosity defects if compared to as-cast from conventional casting [21], [23] and foster a more uniform grain structure, contributing to the mechanical stability of LM25 components, which aligns with trends observed across various casting methods. By adjusting grain size and transforming conventional dendritic structures into semi-solid, globular formations, the cooling slope casting (CSC) process significantly enhances the microstructure of LM25 alloys, resulting in improved strength and ductility [9], [18]. Optimization of CSC parameters has been shown to predictably increase feedstock performance without costly trial-and-error casting experiments [24]. Further improvements in mechanical properties—particularly tensile and impact strength—have been achieved by optimizing process variables such as the slope angle and the addition of grain refiners, especially in Al–7Si–0.3Mg alloys, highlighting the suitability of CSC for thixoforming applications [25], [26].

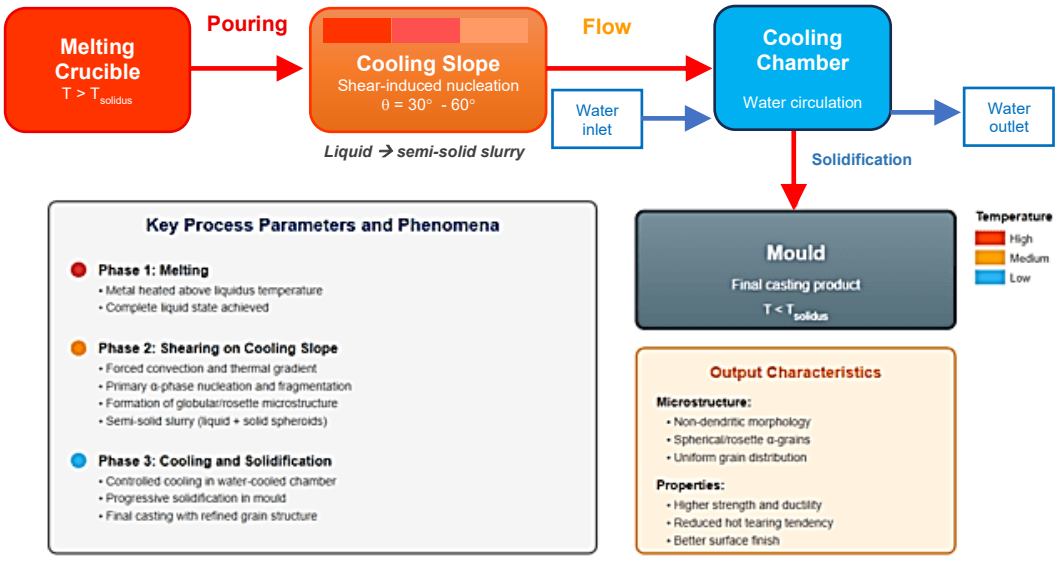

Figure 1. Schematic block diagram of the cooling slope casting facility

1.2 Introduction to Additive Friction Stir Deposition Process

Emerging as a revolutionary additive manufacturing technology, combining the advantages of conventional friction stir welding with additive techniques, is additive friction stir deposition (AFSD). Rotational and translational motions combine in the AFSD process to generate required heat and pressure favourable for proper bonding without melting temperatures [27]. This approach enables components to be built layer by layer, thereby significantly reducing the waste associated with conventional subtractive techniques. It helps metal layers to be deposited in a solid form for materials sensitive to thermal distortion and segregation [28], [29], [30]. Particularly in aerospace applications where weight-to-strength ratios are crucial, the AFSD process greatly improves material use and offers the possibility for repairing damaged components [13], [31]. For example, AFSD has been successfully applied in the repair of structural aluminum components, offering solid-state bonding that minimizes distortion and restores mechanical reliability, which is critical for aerospace applications [32]. The overall AFSD process can be divided into three phases as illustrated in Figure 2. First, the rotating solid consumable feedstock rod advances toward the substrate under axial force, generating frictional heat that plasticizes the material at the rod tip without melting in Phase I (Initial Contact and Heating). For the second phase (Deposition and Layer Formation), the plasticized material is extruded beneath the rotating tool, stirred, and deposited onto the substrate—usually made from the same material—forming a solid bond first layer. The final phase (Multilayer Build-up) involves depositing additional layers by incrementally retracting the tool and guiding it along a defined path after each layer is completed [12]. This solid-state process enables precise control of microstructure and mechanical characteristics during the deposition process through dynamic recrystallization, thus separating AFSD from the traditional fusion-based additive manufacturing approaches.

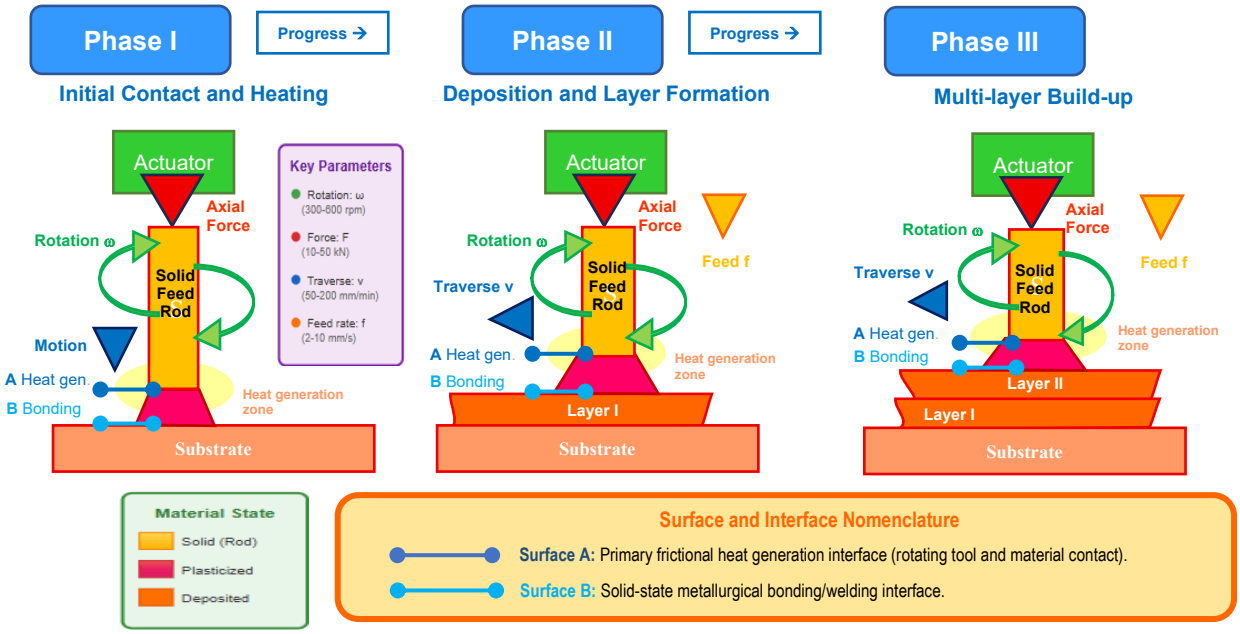

Figure 2. The analogy of entire AFSD process for solid consumable feedstock rod

1.3 Importance of Microstructure and Mechanical Properties of Aluminum Alloys

Maximizing the mechanical performance of the LM25 alloy depends on an awareness of its microstructural development during processing. A variety of techniques have been developed for comprehensive microstructural analysis of LM25 and other aluminum alloys, which is essential for understanding their mechanical behavior. Microstructural characteristics, including grain size, distribution, and phase composition, directly impact the strength, toughness, and ductility of aluminum alloys [33]. The relationships between the microstructure and mechanical characteristics are greatly clarified by characterization methods, including optical microscopy, scanning electron microscopy (SEM) [34], [35], [36], energy-dispersive X-ray spectroscope (EDS) and X-ray diffraction (XRD). Optical and electron microscopy techniques, especially advanced with EDS, offer insights into dimensional characteristics and phase distributions [37], while XRD enables phase identification, critical for fine-tuning the processing parameters [3], [15], [23]. The integration of these methodologies facilitates a robust microstructural characterization framework, allowing for the precise evaluation of the effects of processing conditions on alloy properties. In its as-cast state, LM25 typically exhibits coarse dendritic α-Al grains with an interconnected eutectic Si network, resulting in inconsistent mechanical properties and limited ductility [38]. Cooling slope casting refines this into semi-solid, globular grains, improving homogeneity and flow characteristics—features that enhance the plastic deformation and interlayer bonding needed in AFSD [25]. These results indicate that, despite the observed increases in mechanical properties resulting from separate cooling slope casting and AFSD, the synergistic effects of these processes on the microstructure and mechanical properties of LM25 remain largely uninvestigated. Whether using conventional casting techniques or cutting-edge technologies like AFSD, these revelations help to improve processing approaches.

2. METHODS AND MATERIAL

2.1 Material preparation

The LM25 aluminum alloy was selected as the base material for its exceptional mechanical properties due to its usage in most automotive components, such as vehicle pistons [19], [39], [40]. The spectroscopic investigation of the material was carried out, and its chemical composition is given in Table 1. Three distinct types of samples were prepared for experimentation: as-cast (AC) or permanent mold cast (PMC), cooling slope (CS) cast, and friction stir deposited (FSDed). The AC (1 unit) and CS (3 units) cast samples were then subjected to standard T6 heat treatment according to the American Society for Testing and Materials (ASTM B917). A CS apparatus applied in this study is shown in Figure 3, which consists of an inclined stainless-steel slope plane, a D2 tool steel mold and a portable melting furnace with a graphite crucible. LM25 ingots, after being cut to an appropriate dimension and weighing approximately 200 grams, were melted in the furnace at a superheated temperature of 720°C, followed by cooling to the desired pouring temperature (i.e., 660°C). The molten alloy was poured over a 60° inclined CS plane (surface temperature: 28°C) with a 5 mm thick, 46 mm wide, and 400 mm long plate based on the results of the optimization study conducted by Salleh et al. [9]. Water at room temperature with a flow rate of 2 L/min was circulated underneath the CS plate continuously for 10-15 minutes to ensure an increase in a-Al nucleation along the CS plate [23]. The melt transitioned to a slurry semi-solid state and was collected in a preheated Ø25 X 130 mm cylindrical D2 tool steel mold at 100 °C. The as-cast sample was acquired from the supplier through gravity casting, while the CS cast and FSDed samples were fabricated using the semi-solid processing method and solid-state additive manufacturing approach.

Table 1. Chemical composition of LM25 aluminum alloy

Materials	Weight Percentage (wt.%)
Copper (Cu)	0.2 max
Magnesium (Mg)	0.20-0.60
Silicon (Si)	6.5-7.5
Iron (Fe)	0.5 max
Manganese (Mn)	0.3 max
Nickel (Ni)	0.1 max
Zinc (Zn)	0.1 max
Lead (Pb)	0.1 max
Tin (Sn)	0.05 max
Titanium (Ti)	0.2 max
Aluminum	Remainder

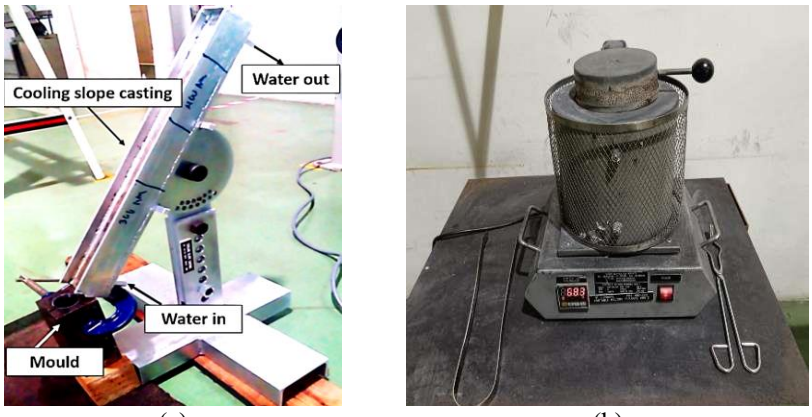

(a) (b)

Figure 3. Cooling slope casting apparatus (a) Cooling slope (CS) with D2 tool steel mold; (b) Portable melting furnace

2.2 T6 Heat Treatment

T6 heat treatment (HT) consists of three steps, which are solution heat treatment, quenching and age hardening (precipitation heat treatment) [8], [9]. All desired billets were subjected to T6 heat treatment based on the ASTM B 917/B 917M – 08 standard (solution treatment at 540°C for 8 hours, water quenching at 65 to 100°C under ambient atmosphere and artificial aging at 160°C for 4 hours) in a Nabertherm oven for heat treatment.

2.3 Additive Friction Stir Deposition (AFSD)

AA LM25 rods were initially cast at ~25 mm diameter using both CSC and PMC methods and then machined to 20 mm diameter to remove the cast surface defect and to fit the AFSD spindle shank setup. The final rods were 80–100 mm

in length, with a usable deposition length of 30–60 mm, which is a straight rod with a flat-ended tip (the rod end with 20 mm diameter acted as the shoulder surface) and were rotated using an FSW spindle with no pin profile. AA6061-T6 sheets (6 × 125 × 240 mm) were used as substrate plates. The deposited tracks were approximately 30–60 mm in length and 3–5 mm in deposit width, as estimated from the deposition setup. Exact deposit dimensions were not systematically measured in this pilot study and are identified as an area for future work. Table 2 provides the chemical composition of AA6061-T6, while Table 1 presents the composition of AA LM25. The AFSD experiments were conducted using a CNC friction stir welding (FSW) machine (Model: HMC 1007-2D, Ningbo Jinfeng Welding and Cutting, China), as illustrated in Figure 4(a). At the beginning of each trial, the AA6061-T6 substrate was firmly fixed onto the machine table, and the prepared AA LM25 rod was placed in the rotating spindle, as illustrated in Figure 4(b). After setting the AFSD process parameters, the AA LM25 rod began rotating and gradually moved downward until it contacted the surface of the secured AA6061 substrate. For this initial investigation, two deposition conditions (400 and 800 rpm, feed 2–3 mm/min) were selected based on prior AFSD literature ranges [10], [15], [17], lab FSW machine experiment experience, and initial trial runs to ensure stable material flow. The friction between the rotating rod and the stationary substrate generated heat, softening the rod and allowing it to deform plastically. As a result, the material was deposited layer by layer onto the AA6061 substrate to form the deposited parts (DPs), as shown in Figure 4(c).

Table 2. Chemical composition of AA6061-T6

Component	Mg	Si	Fe	Cu	Cr	Mn	Zn	Al
Chemical composition (wt. %)	1.014	0.606	0.497	0.233	0.114	0.13	0.111	Bal.

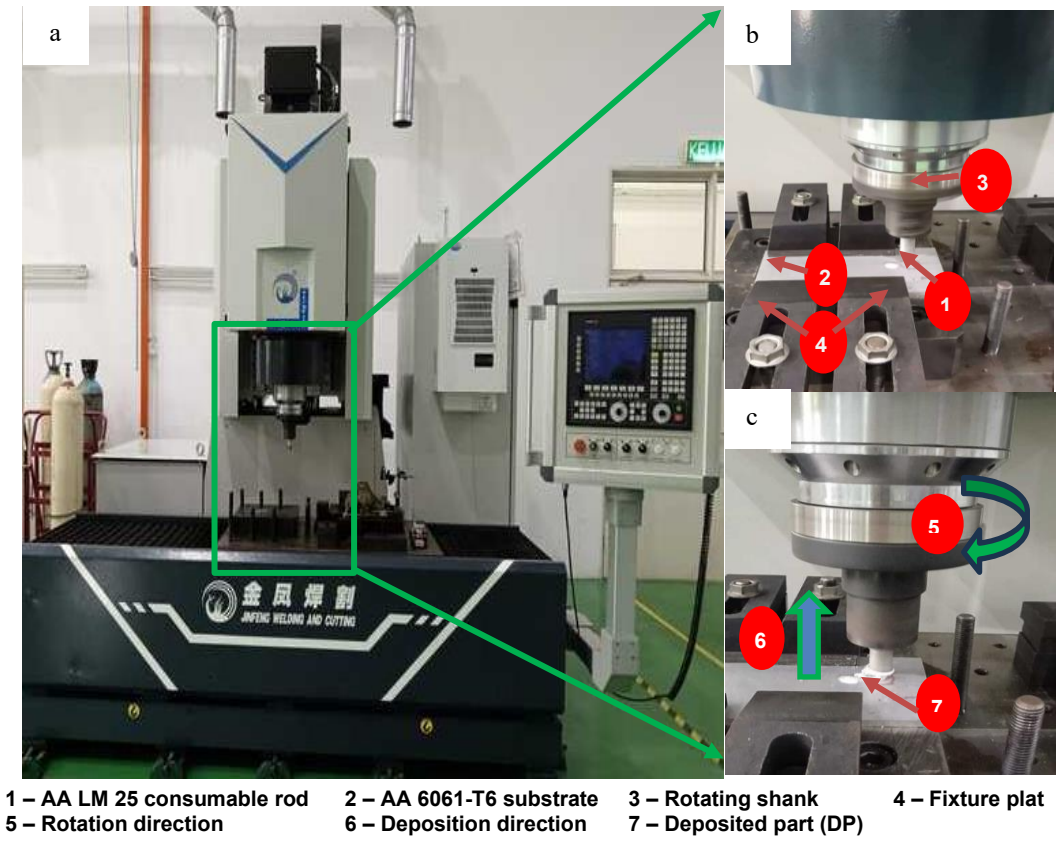

Figure 4. AFSD conducted (a) A CNC FSW machine in UTeM laboratory; (b) setup of the AFSD process of the AA LM25 rod on the AA6061-T6 plate; (c) onset of deposition process

2.4 Sample Preparation and Characterization of the Deposited Parts

Each deposited part (DP) was cross-sectioned at the midpoint along the build direction (z-direction), then cold-mounted and ground using silicon carbide abrasive papers in accordance with metallographic preparation standards. The grinding was done progressively with grit sizes of 240, 400, 600, 800, and 1200 in an average of 3-5 minutes per step. This was followed by polishing with DIAMAT Polycrystalline diamond suspension in three steps—6 µm, 3 µm, and finally 1 µm in an average of 10 minutes per step under ~1-3 N due to manual sample preparation—to achieve a mirror-like surface finish, following ASTM E3 guidelines for macro- and microstructural analysis. The samples were then cleaned using 95% ethanol in an ultrasonic cleaner and etched for 15 seconds using Keller's reagent, as outlined in ASTM E407, to reveal their microstructural features. Microstructure examination was performed on the as-received LM25 rod, the AA6061-T6 substrate, and the AFSD-deposited parts using an optical microscope (Model: Leica DVM6, Leica Microsystems, Singapore) and a scanning electron microscope (Model: SEM SU5000, Hitachi Hi-Tech, Japan) equipped

with an AMETEK energy-dispersive X-ray spectroscopy (EDS) system. This analysis focused on evaluating grain size, grain texture, and silicon particle distribution. Grain size and distribution were measured using ImageJ Analyzer and OriginPro 2025 software, as outlined in ASTM E112, with >500 grains per sample analysed; reported as mean ± SD with minimum/maximum range. Hardness testing was carried out on the LM25 base material and the cross-sectioned DPs using a Vickers hardness tester (Model: FALCON 400G2, INNOVATEST, Netherlands) with a 200 g load and a dwell time of 10 seconds, following ASTM E384. To generate hardness maps, the measured area was divided into five vertical lines with 2 mm spacing between indentations, as illustrated in Figure 5, adapted from prior research [15], [37].

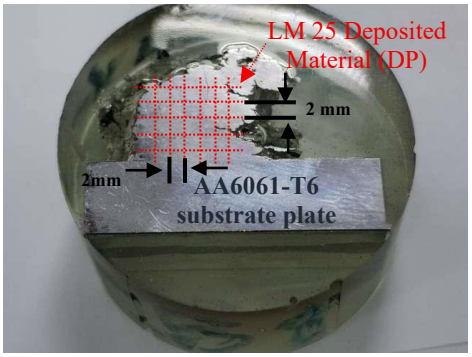

Figure 5. Real specimen diagram showing hardness measurement with grid mapping of the aluminum alloy DP

3. RESULTS AND DISCUSSION

3.1 Macrostructure

To identify the ideal AFSD conditions for additively manufacturing DPs without defects such as broken deposition layers or excessive flash, initial experiments were conducted with this goal in mind. It was observed that rotation speed and the consumable rod's deposition feed rate are critical parameters for AFSD, as also supported by earlier [15], [37], [41], [42]. The rotation speed and feed rate of the consumable rod play a key role in influencing the quality of the deposited parts. Recent research has shown that these two parameters directly affect heat input, which plays a central role in controlling material flow, bonding strength, and the stability of layer formation. Higher rotation speeds or feed rates can lead to excessive softening, while lower values may cause poor bonding due to insufficient heat generation [41], [42].

A moderate rotation speed, such as 400 rpm, combined with a lower feed rate around 3 mm/min, created favourable conditions for fine grain formation through dynamic recrystallisation. This resulted in improved hardness and overall microstructure. Similar trends were reported in studies on AA7075-T6 and A356 alloys, where slower feed rates led to finer grain structures, higher hardness, and more stable, defect-free layer build-up, thanks to well-balanced heat generation and material flow [15], [37]. These observations are further supported by Abbasi-Nahr et al., who reported that using mid-range rotation speeds (800–900 rpm) with feed rates between 5–12 mm/min led to uniform layer bonding, refined grains, and higher hardness in AA5083-based nanocomposites. Their optimized conditions resulted in up to 54% grain size reduction and significantly fewer defects [41], [42].

Conversely, using higher feed rates without adjusting the rotation speed can result in lower heat input, which may cause incomplete bonding, larger grain sizes, or other defects in the deposited layers. However, macrostructure examination of DPs produced at a constant rotational speed of 400 and 800 rpm with deposition feed rates in the Z-direction of 2–3 mm/min has yet to produce defect-free parts, as seen in Figure 6. This figure shows macrographs of the deposited parts alongside their visual appearance with comments. Figures 6a and 6b illustrate discontinuous layer deposition for CSC tools without heat treatment, as the tools broke when the FSW machine was processed at 400 rpm and deposition rates of 2 and 3 mm/min, respectively. Additionally, the AFSD part experienced tearing at a feed rate of 3 mm/min and a rotation speed of 800 rpm (Figure 6(d)). Meanwhile, as shown in Figures 6(c) and 6(e), the DPs processed at deposition feeds of 3 mm/min with a constant rod rotation of 800 rpm demonstrated continuous build-up of AA LM25 layers. Visual examination of the deposit layers indicated that flash accumulated around the LM25 DPs under the applied processing parameters. It appears that heat-treated CSC feedstock produced good results, but further experimental runs are needed to determine optimal process parameters (i.e., RS = 800 rpm or higher; DR = 4 mm/min or higher) for successful multilayer deposition. These findings suggest that although some combinations are promising, further adjustments—such as slightly higher feed rates (e.g. 4 mm/min) and improved tool conditioning—may be necessary to achieve fully defect-free multilayer parts.

Overall, both the researchers' experiment and supporting literature clearly show that achieving high-quality, defect-free layers in AFSD depends heavily on careful balancing of rotation speed and feed rate. Optimizing these parameters not only improves layer bonding and grain refinement but also minimizes surface defects such as voids and flash accumulation [41], [42]. Across all processing parameters, the macrostructure cross-sections of the fabricated DPs tend to show fully continuous structures, but with voids, cracks, and flash defects at the interfaces of the deposited layers, which means they need further adjustment of process parameters in future runs.

3.2 Microstructure Evolution

The as-cast microstructure of the LM25 aluminum alloy, which was first poured directly into the mold after being superheated to 720°C, is displayed in Figure 7. The sample's dendritic microstructure exhibits an uneven shape that is uniformly distributed. A Si-rich eutectic phase (plate-like shape), porosity, primary free-Si, and minor intermetallic phases [15] are dispersed at the α-Al matrix's grain boundaries, encircle the dendritic α-Al arms that make up the microstructure. The average grain size of this as-cast LM25 alloy rod (Figure 7) is 49.68 ± 19.75μm, as determined by the grain interception method using ImageJ software and a microscope.

Consumable tool condition	Visual appearance	Cross-section of the produced LM25 DPs	Remarks
(a) Cooling slope cast tool without heat treatment RS = 400 rpm, DR = 2 mm/min (Denotation: C1) Layer height: 3.5mm	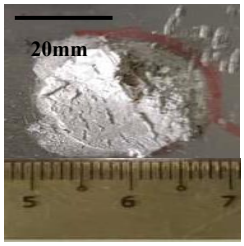		Broken deposition seems like there was initial bonding, but no progressive bonding occurred. **Rejected**
(b) Cooling slope cast tool without heat treatment RS = 400 rpm, DR = 3 mm/min (Denotation: C2) Layer height: 2.5mm	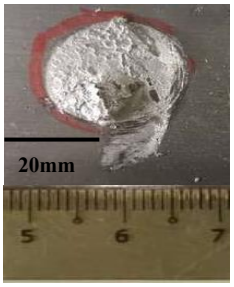		Broken deposition seems like there was initial bonding, but no progressive bonding occurred. **Rejected**
(c) Cooling slope cast tool with heat treatment RS = 800 rpm, DR = 3 mm/min (Denotation: C5) Layer height: 11.5mm	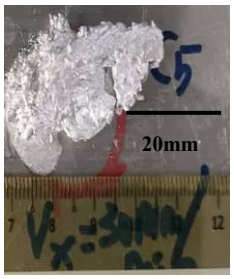	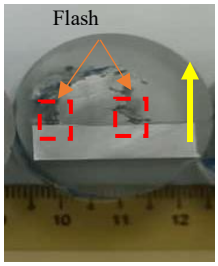	Continuous deposition with one layer and the largest height. Accepted with improvement
(d) Cooling slope cast tool without heat treatment RS = 800 rpm, DR = 3 mm/min (Denotation: C6) Layer height: 2.0mm	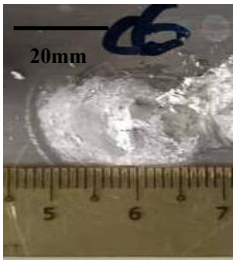	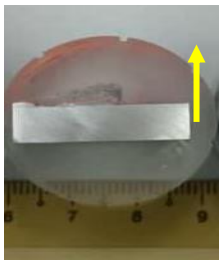	A little deposition with tearing. **Rejected**
(e) As-cast tool with heat treatment RS = 800 rpm, DR = 3 mm/min (Denotation: D2) Layer height: 4.5mm	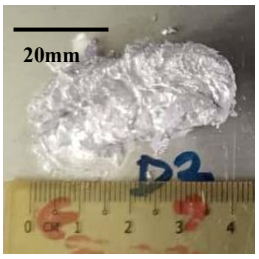	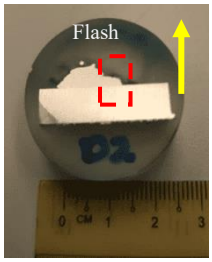	Continuous deposition with one layer. Accepted with improvement

Figure 6. The deposited materials formed by the AFSD technique, processed at different rotation speeds (400-800 rpm) and various feed rates (2-3 mm/min), are enclosed with visual inspection remarks and a cross-section of a macrograph (LM25 DPs)

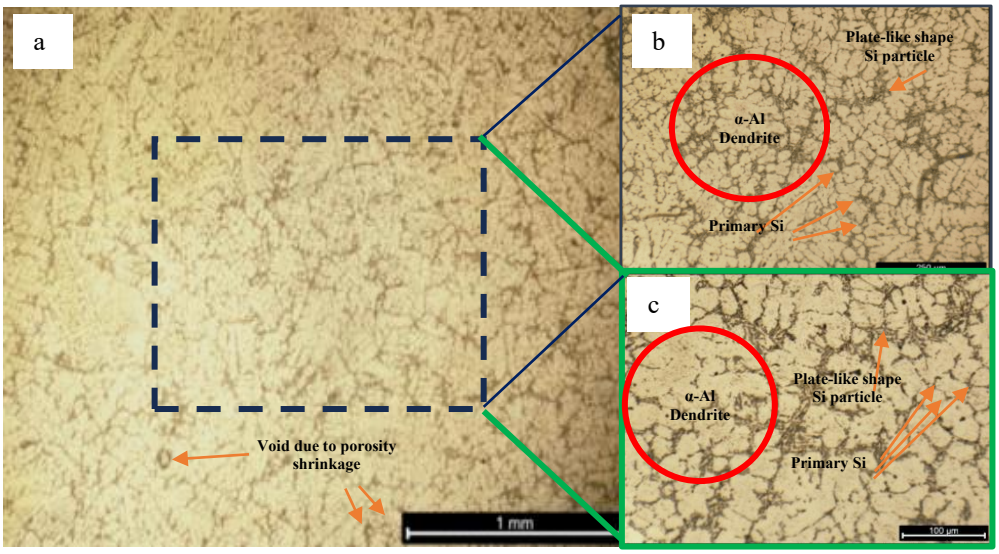

Figure 7. OM images show the microstructure of the consumable tool (a) the as-cast LM25 alloy without heat treatment before use for AFSD, (b, c) at higher magnifications

3.2.1 Microstructure of the Consumable Rod of As-cast and CSC Before AFSD Process

Significant variations in grain size and microstructure morphology are shown in Figure 8 for the hypoeutectic LM25 alloy samples that were AC-cast with heat treatment, CS-cast with heat treatment, AC-cast without heat treatment, and CS-cast with heat treatment. An α-Al phase, Si particles in the eutectic phase, and a variety of minor intermetallic compounds are present in all samples [15], [23]. The AC samples (Figure 8(a) and 8(e)) have circular-shaped Si particles and coarse a-Al dendrites with interdendritic channels that contain the Al–Si eutectic. However, the AC sample without heat treatment shows more microporosities and micro-shrinkage (Figure 8(e) and 8(g)). This is probably because air and oxide film entrapment occurred during mold filling, and the high turbulent flow associated with the solidification stage makes it worse [23]. As shown in Figures 8(a) and 8(c), it appears that the Al-Si eutectic's grain boundaries are not visible following heat treatment.

A non-uniform rosette-like α-Al microstructure encircled by the eutectic phase can be seen in Figure 8(b) and 8(f). Surprisingly, the microstructures were different from the feedstock used for conventional casting, as illustrated in Figures 8(a) and 8(e). The CSC caused the dendritic microstructure to completely change into the non-dendritic microstructure, even though the α-Al grains did not produce a uniform fine globular microstructure. External shear forces along the cooling slope plate in AC alloys cause the dendritic arm to break, which further refines the α-Al matrix. Furthermore, the microstructure's Si phase refines and takes on a comparatively round lamellar shape due to the break-off of primary dendritic arms and minor breaking of secondary dendritic arms [9], [23]. With the assistance of T6 heat treatment, the α-Al globules in the samples' microstructure in Figures 8b and 8d further coarsened. This circumstance was also noted in a study by Hanizam et al. [8] and Anuar et al. [43]. Furthermore, following T6 treatment, most of the plate-like eutectic-Si particles took on a rounded form and became embedded between α-Al globules. During the solution treatment, the T6 treatment changed the eutectic-Si shape, which resulted in the formation of an intergranular contrast during artificial aging [8].

3.2.2 Microstructure of the Deposited Parts after AFSD

For this initial investigation, field emission scanning electron microscopy (FESEM) analysis was employed in addition to OM to thoroughly examine the impact of deposition feed rates and T6 heat treatment on the microstructure characteristics of the AFSD materials. FESEM micrographs paired with OM images of the LM25 DPs generated following successive layers of material deposition at a rate of 3 mm/min are displayed in Figure 9 for the CS cast without heat treatment (Figure 9(a), (b)), the as-cast with heat treatment (Figure 9(c)), and the cs cast with heat treatment (Figure 9(d)). The FESEM image in Figure 9(a) reveals a non-uniform, discontinuous bonding interface between the deposited material and the substrate. The curved interface and broad boundary zone indicate insufficient metallurgical bonding. This failure can be attributed to inadequate heat input or poor material flow since the rotation speed applied for this sample is 400 rpm, which resulted in weak plastic deformation and poor interfacial bonding. In the meantime, the rotation speed of 800 rpm was applied for samples in Figure 9 (b)-(d). Failure in Figure 9(b), which reveals unfilled voids and cracks at the interface, likely caused by insufficient or a mismatch in thermal conductivity due to non-uniform pre-cooling, preventing proper plasticization. In AFSD, material flow and dynamic recrystallization depend significantly on both the tool design and tool parameters, such as rotation speed and feed rate, which directly affect thermal input [44] and are influenced by cooling slope-cast initial structures, thus influencing recrystallized grain size and phase morphology [44], affecting grain refinement and mechanical performance [45] too. As seen in Figures 9(c) and 9(d), the FESEM micrographs demonstrate the significant positive impact of AFSD on the distribution and morphology of eutectic-Si, which converts primary Si plates into finer Si particles, driven by thermal-mechanical effects of the process [46], leading to effective bonding and

successful deposition. However, sample C5, which is CSC HT condition enhanced by moderate pre-cooling via cooling slope, promotes heterogeneous nucleation and suppression of porosity [47]. According to Kinser et al. (2025), cooling-assisted AFSD, including submerged and slope-cooling, can enhance microstructural features like grain refinement and reduce porosity. In contrast to Figures 9(a) and 9(b), Figure 9(d) shows microstructural continuity in bonding and better phase distribution due to dynamic recrystallization and heat generation across layers [48], which provides real-time experimental evidence of the optimal process parameter in terms of the CSC hybrid with AFSD. Table 3 summarizes the findings from Figure 9 based on the study of Cooling Slope-Cast LM25 Aluminum in Additive Friction Stir Deposition (AFSD). This matrix organizes each sample's microstructural and mechanical performance to support analysis and discussion in this section.

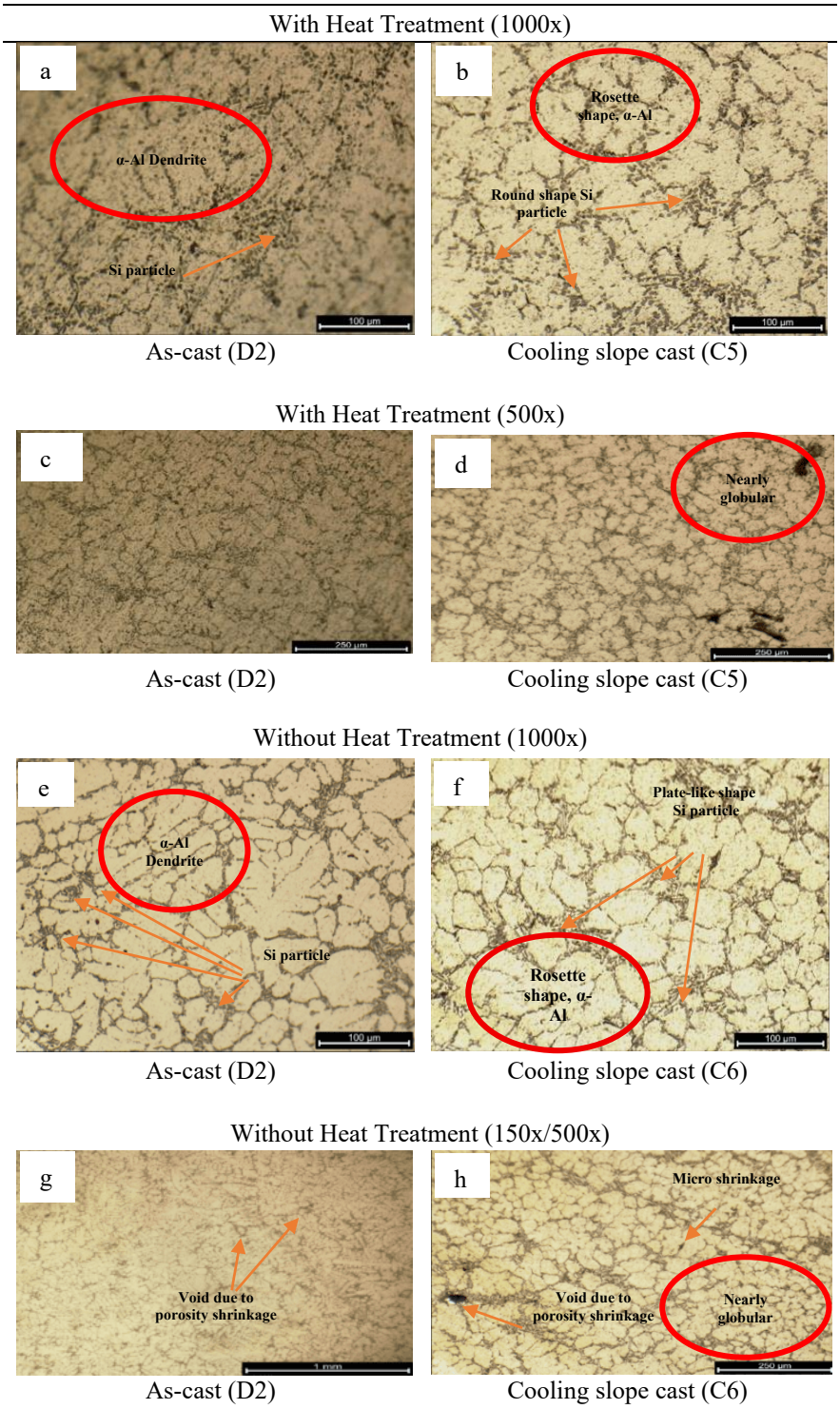

Figure 8. Optical microscopy (OM) images (magnification 500x and 1000x) of hypoeutectic LM25 samples; (a), (c) AC-cast with heat treatment, (b), (d) CS cast with heat treatment (C5), (e), (g) AC-cast without heat treatment, and (f), (h) CS cast with heat treatment (C6)

Determining the size of the α-Al grains was very challenging. Following the friction stir deposition (FSD) process, α-Al grain boundaries become indistinct due to grain refinement and dynamic recrystallization, as confirmed by OM and FESEM analyses[15], [49]. The stir zone in FSP mirrors the thermomechanical zone in AFSD, with similar microstructural evolution [15], [49]. FSP breaks down plate-like Si particles into finer, more uniformly distributed forms and eliminates porosity [15], [49], in addition to what was anticipated for heat-treated samples. These findings align with the improved homogeneity and mechanical properties observed in AFSD-processed A356 alloy in a study of Alzahrani et al. (2021) [15], [49]. By using ImageJ analysis, it is noted that the mean values of the grain size of the produced DPs under varying conditions of consumable rod conditions were 1.828 µm (range: 0.351 - 60.835 µm) for C5 CSC HT, 1.868 µm (range: 0.703 - 30.753 µm) for D2 PMC HT, and 2.390 µm, (range: 0.702 - 35.462 µm) for C6 CSC, respectively, compared to the grain size value of 49.52 ± 28.19 µm for the as-cast alloy (D2). The dynamic recrystallization (DRX) that takes place during the AFSD process is responsible for this extreme grain refinement. Regardless of the initial state of the feedstock, the strong plastic deformation and frictional heat produced by the rotating tool provide favourable conditions for both continuous and discontinuous DRX, resulting in the formation of fine, equiaxed grains [44]. To put it simply, heat-treated feedstocks encourage complete and more uniform recrystallization, which leads to smaller grains, whereas non-heat-treated CSC feedstock (C6) may undergo partial or irregular recrystallization because of its initial microstructure's inhomogeneity. Furthermore, non-heat-treated CSC's residual stresses and uneven particle distribution might prevent uniform grain refinement, resulting in somewhat larger grain sizes in the DP.

Table 3. Summary of FESEM/OM Observations for LM25 DPs in AFSD at 3 mm/min

Sample ID	Deposition Status	Interface Quality	Grain Morphology	Mechanical Performance Implications	Key Microstructural Indicator
C2	Deposition failed	Poor bonding, curve-shaped	Irregular, scattered, coarse	Weak adhesion, high porosity risk	Discontinuous interface; low recrystallization
C6	Deposition failed	Poor bonding, voids/ cracks	Discontinuous and porous regions	Likely brittle; tensile/ fatigue failure zones	Voids at interface; minimal grain refinement
D2	Successful	Continuous, well-bonded	Fine, uniform grains	Good in hardness; reliable bonding	Evidence of dynamic recrystallization
C5	Successful	Strong metallurgical bonding	Dense, equiaxed, refined	Excellent joint quality; improved mechanical traits	Plastic deformation zones, consistent particle dispersion

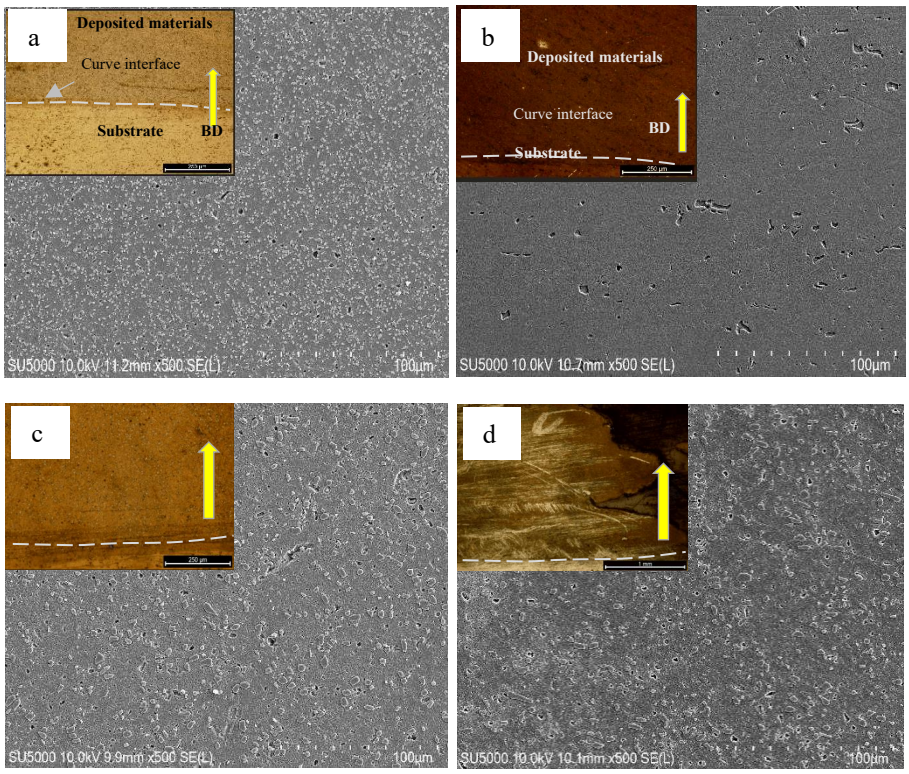

Figure 9. FESEM images attached with Optical microscopy (OM) of hypoeutectic LM25 DPs processed at deposition rate of 3mm/min under varying conditions of samples; (a) C2 (deposition fail), (b) C6 (deposition fail), (c) D2, (d) C5

Figures 10 and 11 support the observed microstructural refinement following AFSD. The EDS mapping and FESEM analyses show a more uniform and fine distribution of elements, particularly Si, across both the deposited part (C5 DP sample) and the tool (C5 CSC HT). This confirms the dissolution of coarse phases and redistribution of alloying elements, aligning with the reduction in visible α-Al grain boundaries due to dynamic recrystallization and plastic flow [15], [49]. The Si mapping in both figures reveals a transition from coarse plate-like particles to smaller, more homogeneously dispersed ones, consistent with prior FSP observations on A356 [40]. This reinforces the similarity between FSP stir zones and AFSD thermomechanical zones [50], [51], both characterized by severe deformation and localized thermal input. Additionally, the even elemental spread seen in the overlay maps and EDS spectra aligns with Jalilvand et al.'s findings that friction-based processing promotes microstructural homogeneity and reduces porosity [52].

Importantly, a finer and more uniform Si distribution observed in CSC-derived deposits compared to PMC deposits is beneficial for mechanical performance, since it aids load transfer and delays crack initiation under stress [10]. Nonetheless, the repeated thermal cycles during AFSD encouraged Si coarsening, which diminished its strengthening contribution and explains part of the hardness reduction observed. Therefore, the redistribution of Si observed in the EDS maps is not only indicative of microstructural refinement but also explains the subsequent hardness response: finer Si promotes load transfer and bonding, while coarsening during repeated thermal cycles diminishes strengthening, as further detailed in Section 3.3

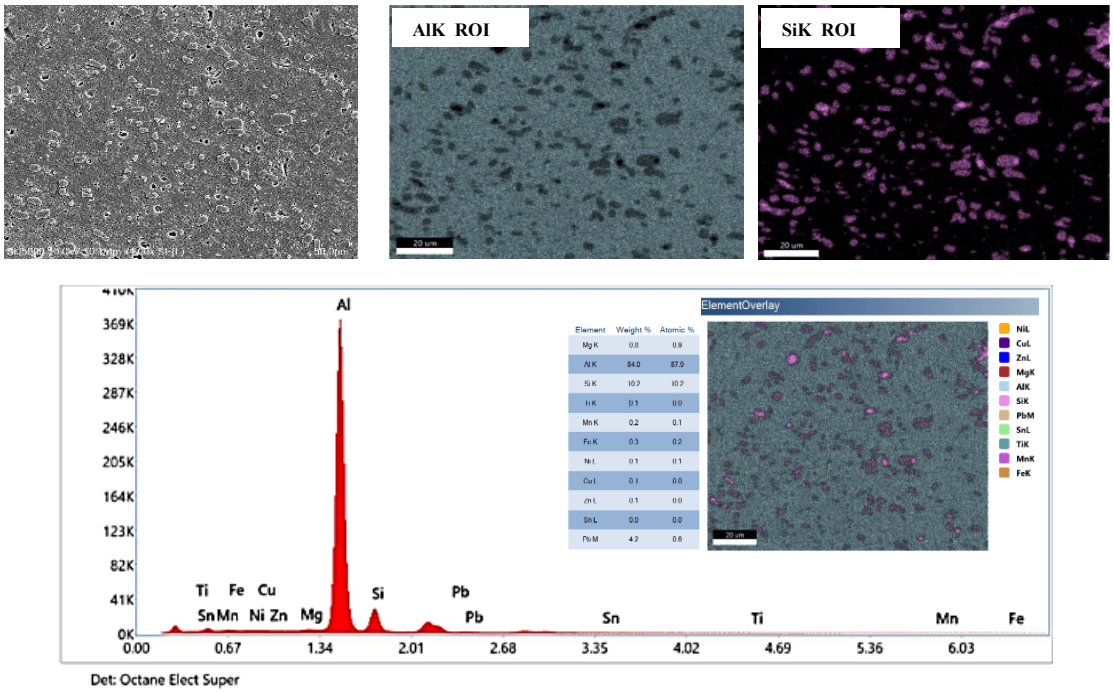

Figure 10. FESEM analysis at 1000x magnification and EDS mapping results reveal the elemental distribution of the C5 DP sample after deposition using the CSC HT consumable tool

3.3 Mechanical Property: Hardness Results

The hardness profiles in Figure 12 and the average hardness values in Figure 13, when viewed together with the microstructure images in Figure 9, help explain how AFSD and feedstock type influence the mechanical behaviour of LM25 aluminum alloy. Figure 12 presents the Vickers hardness measured at different heights along the deposited parts (DPs), revealing how hardness varies layer by layer. The hardness variation layer-by-layer in Figure 12 highlights this behaviour, reflecting changes in thermal exposure and plastic flow during deposition, which affect the grain structure. Among the samples, D2 PMC_HT and C5 CSC_HT showed relatively steady hardness values across the build height, while others like C2 and C6 had more noticeable fluctuations—likely due to uneven heat input or inconsistent structure across layers. As shown in Figure 13, even though all deposited samples displayed good bonding without visible defects (see Figure 9(c)-(d)), their hardness values were lower than those of the original base materials (BMs). For example, C5 CSC_HT dropped from 80.28 HV in the rod to 67.07 HV after deposition, and D2 PMC_HT also fell from 79.08 HV to 67.14 HV. These drops in hardness are likely due to thermal softening and the over-aging of strengthening particles such as Mg_2Si, caused by the repeated heating during the AFSD process [27], [45]. The hardness of the deposited parts decreased from approximately 89 HV in the base LM25 to 63–72 HV, representing a reduction of roughly 20–29%. This decline is mainly linked to the repeated heating and cooling that occur during the AFSD process. These thermal cycles cause Mg_2Si precipitates to overage, eutectic Si particles to grow larger, and the aluminum matrix to undergo recovery and partial recrystallization. Together, these changes lower the dislocation density and weaken the precipitation hardening effect, which are normally key contributors to the strength of Al–Si–Mg alloys [15], [16]. As a result, although AFSD helps refine grains through intense plastic deformation, the benefits of grain refinement are outweighed by thermal softening, explaining the overall loss in hardness.

Even though both C5 (CSC_HT) and D2 (PMC_HT) samples underwent T6 heat treatment, C5 displayed more stable deposition behaviour and slightly higher hardness. This improvement can be attributed to the refined, globular grains formed through CSC, which enhanced material flow, reduced porosity, and promoted stronger bonding with the substrate [18], [19]. By comparison, the PMC feedstock retained a coarser dendritic structure, restricting plastic flow during deposition and leading to a weaker mechanical response. This demonstrates that CSC contributes not only to grain refinement but also to interfacial bonding during AFSD, giving it advantages beyond hardness alone.

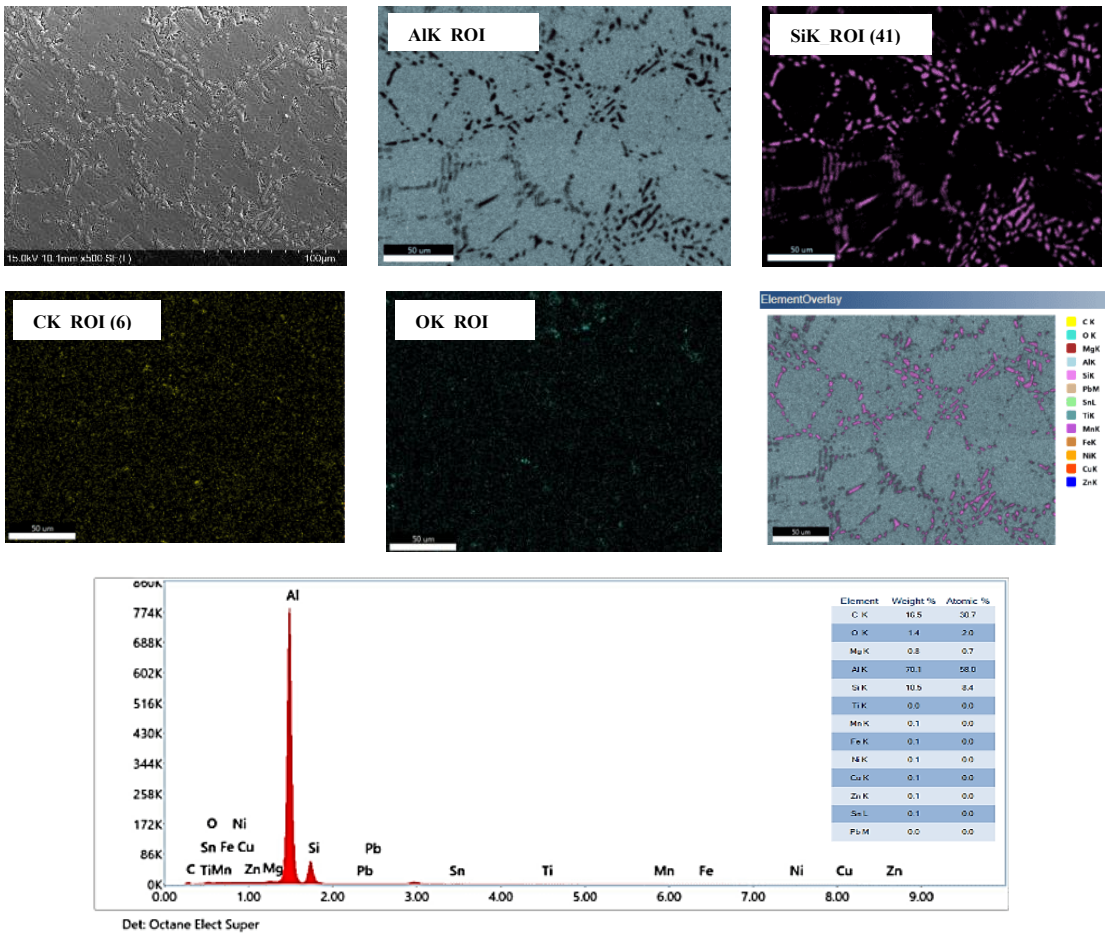

Figure 11. FESEM analysis at 500x magnification and EDS mapping results show the elemental distribution of the C5 CSC HT consumable tool after use for deposition

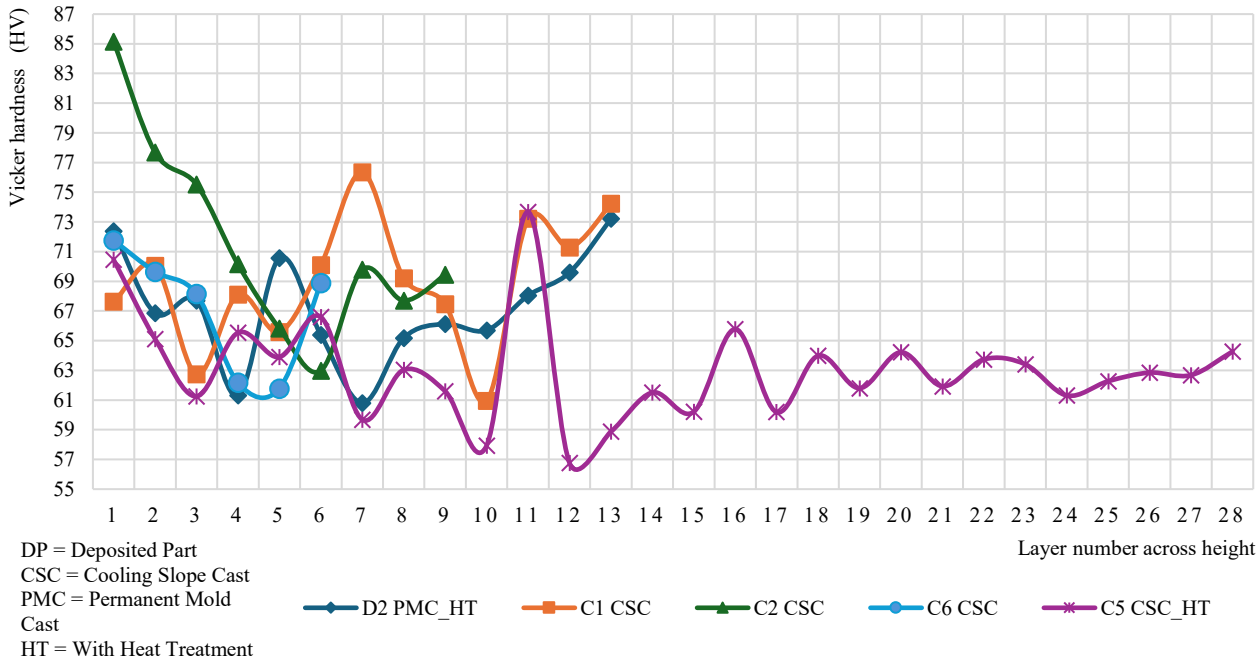

Figure 12. The hardness profile according to layer height of cross-sectioned DPs under various sample conditions.

Although CSC-based samples show lower post-deposition hardness, this is not necessarily detrimental. A softer feedstock can improve plastic flow and facilitate better layer bonding. As reported by Zhang et al. (2025), interfacial bonding during AFSD is highly dependent on feedstock deformability and grain flow at the interface, both of which are enhanced in CSC feedstocks due to their globular microstructure and semi-solid characteristics [53]. The researchers showed that elemental redistribution, such as Zn enrichment at the 7075/2024 interface, suppressed grain growth and enhanced shear strength in multilayer AFSD deposits. Likewise, Dong et al. (2025) reported that optimized AFSD parameters refined grains and promoted uniform precipitate distribution at interfaces, directly improving bonding and strength [54]. Even though the deposited parts showed an overall drop in hardness, the CSC feedstock still performed better than the PMC rods in terms of bonding and deposition quality. The more globular and refined grains created during CSC made the material easier to deform plastically during AFSD, which helped improve flow and contact at the interface. As a result, the deposited layers were smoother and showed fewer visible issues such as porosity or weak bonding [20]. This indicates that, despite the hardness loss caused by thermal cycles, CSC feedstock offers clear process advantages by enhancing deposition reliability and structural soundness, making it a stronger option compared to conventionally cast rods. Together, these studies confirm that microstructural refinement and elemental homogenization play a critical role in bonding quality. By analogy, CSC-derived feedstock enhances interfacial bonding in LM25 through improved plastic flow and more uniform Si distribution, even though thermal cycles still reduce hardness. Thus, while thermal softening may reduce hardness, CSC feedstock still supports strong, defect-free bonding, making it advantageous for certain AFSD applications.

In summary, AFSD provides good layer bonding due to dynamic grain changes and plastic flow, but it does not always preserve strength. To achieve both strength and bonding, it's important to improve feedstock structure and fine-tune processing settings. One possible solution is to use thixoforming on CSC feedstock, which creates more uniform, rounded grains that respond better to ageing [55]. Another option is to apply a post-deposition ageing process to restore strength by allowing the reformation of hardening phases [48].

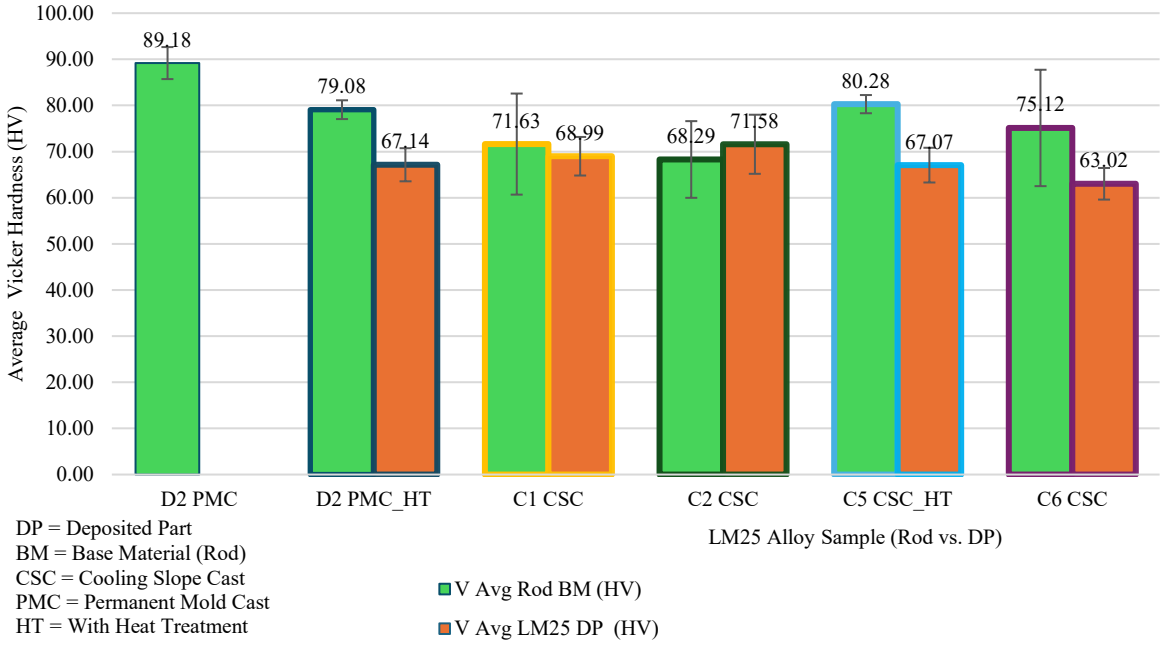

Sample	V Avg Rod BM (HV)	SD Rod BM (HV)	V Avg LM25 DP (HV)	SD LM25 DP (HV)
D2 PMC	89.18	3.47		
D2 PMC_HT	79.08	2.03	67.14	3.59
C1 CSC	71.63	10.95	68.99	4.18
C2 CSC	68.29	8.31	71.58	6.40
C5 CSC_HT	80.28	1.97	67.07	3.77
C6 CSC	75.12	12.61	63.02	3.42

Figure 13. Comparison of average Vickers hardness between LM25 rods and deposited parts across feedstock conditions

4. CONCLUSIONS

This study investigated the feasibility of fabricating LM25 aluminum alloy deposited parts (DPs) on an AA6061-T6 substrate using Additive Friction Stir Deposition (AFSD). The feedstock was prepared by cooling-slope casting (CSC)

and T6 heat treatment. Macrostructural inspection, microstructural analysis, and hardness testing were conducted to assess the effects of rotational speeds (400 and 800 rpm) and deposition feed rates (2–3 mm/min). Based on the analysis of the results, the following conclusions can be drawn:

- The original microstructure of LM25 was notably modified by the semi-solid process, specifically cooling-slope casting (CSC), reducing the grain size to approximately 1.87 ± 1.63 μm and transformed coarse dendritic grains into more globular forms. This structural enhancement suggests that CSC feedstock may provide benefits in nucleation and flow behaviour during AFSD.
- CSC heat-treated rods enabled continuous, though not yet defect-free, deposition at 800 rpm and 3 mm/min. However, further work and experimental validation are necessary to identify optimal process parameters for achieving multilayer deposition while maintaining mechanical integrity, especially for CSC-derived feedstock.
- Despite successful deposition, all parts, regardless of whether they were produced from PMC or CSC feedstocks, exhibited a consistent reduction in hardness compared to their respective base materials. This decline is attributed to heat softening effects, such as potential over-aging and precipitate coarsening during AFSD.

This study confirms that CSC feedstock is feasible for AFSD and enables smooth, continuous deposits. However, hardness retention remains a limitation, especially with CSC LM25 alloy feedstock. Future efforts should focus on improving feedstock quality (e.g., through thixoforming), reducing thermal degradation during deposition, and investigating post-AFSD heat treatments to restore strength. Future work should also include systematic measurement of deposit dimensions to better correlate AFSD process parameters with deposition geometry and mechanical properties. These avenues are vital to broadening AFSD's industrial potential by enabling the manufacture of high-performance aluminum alloy parts for the automotive and aerospace industries.

Based on the findings and goals of this pilot study, the following practical recommendations are provided to guide future research aimed at improving AFSD of LM25 alloy via CSC feedstock:

i) Enhance feedstock quality through thixoformed CSC with T6 treatment. Thixoforming can substantially improve the microstructure of CSC LM25 by promoting spheroidization of α-Al and refining eutectic Si, resulting in a more uniform, globular structure with reduced porosity. Post-thixoforming T6 treatment further dissolves coarse intermetallics and precipitates strengthening phases, thereby improving feedstock consistency, response to thermal-mechanical cycles during AFSD, and, ultimately, hardness in DPs.

ii) Reassess and optimize AFSD parameters. Researchers should consider lower rotational speeds and carefully selected feed rates to minimize overheating and over-aging caused by excessive thermal cycles, which reduce hardness. As supported by Kinser et al. (2025) and Zhu et al. (2024), submerged AFSD and controlled deposition energy, along with in-situ cooling techniques such as water mist or submerged AFSD, are proven to enhance hardness and microstructure retention and limit thermal degradation.

iii) Implement post-AFSD T6 Heat Treatment. If thermal cycles during deposition diminish hardness, applying a post-deposition T6 treatment may restore or enhance mechanical strength by reprecipitating Mg_2Si and refining the microstructure. This approach has been highly successful in other aluminum alloys such as 6061 and 7075. The study by Chen et al. (2023) indicates that post-AFSD T6 treatment can restore, and sometimes surpass, the original material properties.

ACKNOWLEDGEMENTS

The authors would like to thank Universiti Teknikal Malaysia Melaka (UTeM) for financial support under the research grant FRGS/1/2023/TK10/UTEM/02/3 and UTeM Kesidang Scholarship. The authors also extend gratitude to all the technical staff of Fakulti Teknologi dan Kejuruteraan Industri dan Pembuatan, UTeM, for their invaluable assistance in conducting the experiments and collecting data, which were essential to the success of this research.

CONFLICT OF INTEREST

The authors declare that there is no conflict of interest.

AUTHORS CONTRIBUTION

S.C. Tham: Perform Conceptualization, Methodology, Literature Review, Experiment and Analysis, and Manuscript Writing – Original Draft.

M.K. Sued: Contributed to Conceptualization, Methodology, Visualization, Supervision, Manuscript Writing, Review, and Editing.

M.S. Salleh: Involved in Casting Technique Technology Supervision and Review on Material Analysis Theory.

N.I.S. Hussein: Supervision in Empirical Work and Review of the Manuscript.

A. S. Anuar: Involved in Welding Process, Heat Treatment and Data Curation.

M. M. Abdulatef: Contribute to Process Casting Monitoring and Welding Process.

R. Muslim: External advisor for Empirical Work Idealization.

REFERENCES

[1] H. Ravinath, I. I. Ahammed, P. H., S. A. Devan., V R. A. Senan, K.V. Shankar, et al., "Impact of aging temperature on the metallurgical and dry sliding wear behaviour of LM25 / Al2O3 metal matrix composite for potential automotive application," *International Journal of Lightweight Materials and Manufacture*, vol. 6, no. 3, pp. 416–43, 2023.

[2] P. Suresh, P. Arunagiri, and A. P. Arun Pravin, "Experimental analysis of aluminium alloy LM25 with carbon in composite material," in *Materials Today: Proceedings*, Elsevier, Jan 2020, pp. 7–12.

[3] K. Surani, M.V. Galindo, H. Patel, V.I. Velkin, M.I. Haque Siddiqui, A. Kumar, et al., "Effect of copper addition on mechanical properties and microstructures of LM25 cast alloys," *AIP Advances,* vol. 14, no. 4, p. 045025, 2024.

[4] K. Sunitha, K. Gurusami, N. Rajeswari, A. Kathikraja, and L. Saravanan, "Investigation of mechanical properties of SiC particle reinforced Aluminium A356 / LM25 alloy composite," in *Materials Today: Proceedings*, Elsevier Ltd, Jan. 2022, pp. 1983–1987.

[5] M. Zhang, F.C. Liu, Z.Y. Liu, P. Xue, P. Dong, H. Zhang, et al., "Highly stable nanoscale amorphous microstructure at steel-aluminum interface enabled by a new solid-state additive manufacturing method," *Scripta Materialia*, vol. 227, p. 115300, 2023.

[6] J. Liu, Y. Miao, R. Wu, C. Wei, Y. Zhao, Y. Wu, et al., "Effect of heat treatment on microstructure, mechanical properties and corrosion resistance of 7075 aluminum alloys fabricated by improved friction stir additive manufacturing," *Journal of Alloys and Compounds*, vol. 1007, p. 176512, 2024.

[7] F. Liu, P. Dong, A.S. Khan, Y. Zhang, R. Cheng, A. Taub, et al., "3D printing of fine-grained aluminum alloys through extrusion-based additive manufacturing: Microstructure and property characterization," *Journal of Materials Science & Technology*, vol. 139, pp. 126–136, 2023.

[8] H. Hanizam, M. S. Salleh, M. Z. Omar, A. B. Sulong, and M. A. M. Arif, "Effects of hybrid processing on microstructural and mechanical properties of thixoformed aluminum matrix composite," *Journal of Alloys and Compounds*, vol. 836, p. 155378, 2020.

[9] M. S. Salleh, H. Hashim, M.Z. Omar, A.B. Sulong, S. Abd Rahman, S.H. Yahaya, et al., "T6 heat treatment optimization of Thixoformed LM4 aluminium alloy using response surface methodology," *Malaysian Journal on Composites Science and Manufacturing*, vol. 3, no. 1, pp. 1–13, 2020.

[10] Z. McClelland, K. Dunsford, B. Williams, H. Petersen, K. Devami, M. Weaver, et al., "Microstructure and mechanical behavior comparison between cast and additive friction stir-deposited high-entropy alloy Al0.35CoCrFeNi," *Materials*, vol. 17, no. 4, p. 910, 2024.

[11] E. Yasa, O. Poyraz, A. Molyneux, A. Sharman, G. M. Bilgin, and J. Hughes, "Systematic review on additive friction stir deposition: Materials, processes, monitoring and modelling," *Inventions,* vol. 9, no. 6, 2024.

[12] R. S. Mishra, R. S. Haridas, and P. Agrawal, "Friction stir-based additive manufacturing," *Science and Technology of Welding and Joining*, vol. 27, no. 3, pp. 141–165, 2022.

[13] J. Shao, A. Samaei, T. Xue, X. Xie, S. Guo, J. Cao, et al., "Additive friction stir deposition of metallic materials: Process, structure and properties," *Mater Des*, vol. 234, 2023.

[14] R. J. Griffiths, A. E. Wilson-Heid, M. A. Linne, E. V. Garza, A. Wright, and A. A. Martin, "Additive friction stir deposition of a tantalum–tungsten refractory alloy," *Journal of Manufacturing and Materials Processing*, vol. 8, no. 4, p. 177, 2024.

[15] B. Alzahrani, M.M.E.S. Seleman, M.M.Z. Ahmed, E. Elfishawy, Ahmed, A.M.Z., Touileb, K., et al., "The applicability of die cast A356 alloy to additive friction stir deposition at various feeding speeds," *Materials*, vol. 14, no. 20, p. 6018, 2021.

[16] J. J. S. Dilip and G. D. Janaki Ram, "Microstructure evolution in aluminum alloy AA 2014 during multilayer friction deposition," *Materials Characterization*, vol. 86, pp. 146–151, 2013.

[17] V. Soni, R.L. Menchaca, D. Davis, N.N. Kumar, M. Gonzalez, P. Awasthi, et al., "Process-specific design strategy enables exceptional as-deposited strength-ductility synergy in novel Al–Ce alloys via additive friction stir deposition (AFSD)," *Journal of Materials Research and Technology*, vol. 35, pp. 1889–1900, 2025.

[18] M. Jahanbakhshi, S. Nourouzi, R. Naseri, and K. Esfandiari, "Investigation of simultaneous effects of cooling slope casting and mold vibration on mechanical and microstructural properties of A356 aluminum alloy," *Metals and Materials International*, vol. 28, no. 6, pp. 1508–1516, 2022.

[19] D. K. Yadav and I. Chakrabarty, "Effect of cooling slope casting and partial remelting treatment on microstructure and mechanical properties of A319-xMg2Si In-Situ composites," *Materials Science and Engineering: A*, vol. 791, p. 139790, 2020.

[20] M. A. H. Safian, M. S. Salleh, S. Subramonian, N. I. S. Hussein, M. A. Sulaiman, and S. H. Yahaya, "Production of LM4 feedstock for thixoforming using cooling slope casting," *Journal of Advanced Manufacturing Technology*, vol. 11, no. 1, pp. 77–90, 2017.

[21] Z. Li, Y. Li, R. Zhou, L. Xie, Q. Wang, L. Zhang, et al., "Microstructure and properties of semi-solid 7075 aluminum alloy processed with an enclosed cooling slope channel," *Crystals (Basel)*, vol. 13, no. 7, p. 1102, 2023.

[22] H. A. Ibrahim and M. M. Saeed Mulapeer, "Semi-solid casting of aluminum alloy using a cooling slope technic," *Zanco Journal of Pure and Applied Sciences*, vol. 32, no. 3, pp. 49–56, 2020.

[23] S. Samat, M. Z. Omar, I. F. Mohamed, A. H. Baghdadi, and A. M. Aziz, "A comparative study on microstructure, mechanical property and damping capacity of hypoeutectic Al–Si–Cu alloy for different casting technologies," *International Journal of Metalcasting*, vol. 19, no. 2, pp. 1180-1193, 2024.

[24] R. M. Said, M. R. M. Kamal, N. H. Hussin, S. M. Suhaili, S. H. H. Anuar, A. Samsuddin, et al., "Modeling and prediction of the mechanical properties of feedstock by cooling-slope casting process using MOJaya algorithm," *Journal of Advanced Research in Applied Mechanics*, vol. 121, no. 1, pp. 13–26, 2024.

[25] P. Das, "Microstructure and mechanical properties of cooling slope rheocast Al-7Si-0.3Mg alloy and development of a rheo pressure die cast knuckle housing," *Metallurgical and Materials Transactions B: Process Metallurgy and Materials Processing Science*, vol. 54, no. 1, pp. 395–424, 2023.

[26] T. Tugiman, A. Thayab, F. Ariani, T. Sitorus, S. Suhandi, and R. Rizki, "The Effect of Cooling Slope on Mechanical Properties of Aluminum-8.5wt.% Si Alloy Produced by Gravity Casting," in *Proceedings of the 2nd Annual Conference of Engineering and Implementation on Vocational Education (ACEIVE 2018), 3rd November 2018, North Sumatra*, 2019.

[27] L. Chen, L. Zhu, L. Lu, Z. Yang, X. Ren, and X. Zhang, "The effect of heat treatment on the microstructure and electrochemical corrosion behavior of multilayer AA6061 alloy fabricated by additive friction stir deposition," *Applied Surface Science*, vol. 650, p. 159167, 2024.

[28] E. Yasa, O. Poyraz, K. Do, A. Molyneux, J. McManus, and J. Hughes, "In-situ monitoring and control of additive friction stir deposition," *Materials*, vol. 18, no. 7, p. 1509, 2025.

[29] Q. Qiao, M. Zhou, X. Gong, S. Jiang, Y. Lin, H. Wang, et al., "In-situ monitoring of additive friction stir deposition of AA6061: Effect of layer thickness on the microstructure and mechanical properties," *Additive Manufacturing*, vol. 84, p. 104141, 2024.

[30] M. Zhang, T. Jiang, X. Feng, Y. Xie, Y. Su, Z. Sun, et al., "Investigation on in-situ tensile behaviors of 6061 aluminum alloy fabricated by wire additive friction stir deposition," *Journal of Alloys and Compounds*, vol. 1008, p. 176780, 2024.

[31] N. Gotawala and H. Z. Yu, "Material flow path and extreme thermomechanical processing history during additive friction stir deposition," *Journal of Manufacturing Processes*, vol. 101, pp. 114–127, 2023.

[32] L. P. Martin, A. Luccitti, and M. Walluk, "Repair of aluminum 6061 plate by additive friction stir deposition," *International Journal of Advanced Manufacturing Technology*, vol. 118, no. 3–4, pp. 759–773, 2022.

[33] M. M. Z. Ahmed, M. M. El-Sayed Seleman, E. Ahmed, H. A. Reyad, N. A. Alsaleh, and I. Albaijan, "A novel friction stir deposition technique to refill keyhole of friction stir spot welded AA6082-T6 dissimilar joints of different sheet thicknesses," *Materials*, vol. 15, no. 19, p. 6799, 2022.

[34] D. Traiano, S. do Nascimento Rosa, L. A. Lourençato, A. Sánchez Roca, M. C. Sánchez Orozco, and H. D. Carvajal Fals, "Multiresponse optimization applied to friction-stir processing to enhance wear and corrosion performance in Al–Si alloys," *Discover Applied Sciences*, vol. 6, no. 12, p. 643, 2024.

[35] Z. Shen, M. Zhang, D. Li, X. Liu, S. Chen, W. Hou, et al., "Microstructural characterization and mechanical properties of AlMg alloy fabricated by additive friction stir deposition," *International Journal of Advanced Manufacturing Technology*, vol. 125, no. 5–6, pp. 2733–2741, 2023.

[36] A. I. Abdel-Aziz, A. S. A. A. Taleb, Z. M. El-Baradie, and A. I. Z. Farahat, "Effect of friction stir processing on the microstructure and mechanical properties of A384 aluminum alloy," *Key Engineering Materials*, vol. 786, pp. 23–36, 2018.

[37] Y. G. Y. Elshaghoul, M.M. El-Sayed Seleman, A. Bakkar, S.A. Elnekhaily, I. Albaijan, M.M.Z. Ahmed, et al., "Additive friction stir deposition of AA7075-T6 alloy: Impact of process parameters on the microstructures and properties of the continuously deposited multilayered parts," *Applied Sciences (Switzerland)*, vol. 13, no. 18, p. 10255, 2023.

[38] P. Vijayavel, V. Balasubramanian, and I. Rajkumar, "Effect of tool traverse speed on strength, hardness, and ductility of friction-stir-processed LM25AA-5% SiCp metal matrix composites," *Metallography, Microstructure, and Analysis*, vol. 7, no. 3, pp. 321–333, 2018.

[39] M. R. S. Ganesh, N. Reghunath, M. J.Levin, A. Prasad, S. Doondi, and K. V. Shankar, "Strontium in Al–Si–Mg Alloy: A Review," *Metals and Materials International*, vol. 28, no. 1, pp. 1–40, 2022.

[40] S. Vellingiri, "An experimental and investigation on the micro-structure hardness and tensile properties of Al-GrFe3O4 hybrid metal matrix composites," *FME Transactions*, vol. 47, no. 3, pp. 511–517, 2019.

[41] M. Abbasi-Nahr, S. E. Mirsalehi, and S. S. Mirhosseini, "Additive manufacturing of AA5083/TiN-Diamond hybrid nanocomposite parts via additive friction stir deposition: Metallurgical structure, mechanical, tribological, and electrochemical properties," *Journal of Materials Research and Technology*, vol. 30, pp. 8187–8208, 2024.

[42] M. Abbasi–Nahr and S. E. Mirsalehi, "Additive friction stir deposition of AA5083/MoS2-diamond hybrid nanocomposites: Investigating their metallurgical, mechanical, tribological, and electrochemical characteristics, and process-structure-property relationships," *Journal of Alloys and Compounds*, vol. 1013, 2025.

[43] N. F. B. W. Anuar, M. S. Salleh, M. Z. Omar, W. F. H. W. Zamri, S. H. Y. Yahaya, and A. M. Ali, "Effect of T6 heat treatment on microstructure and hardness properties of thixoformed graphene-reinforced A356 composites," *Journal of Advanced Manufacturing Technology*, vol. 17, no. 1, pp. 73–85, 2023.

[44] X. Feng, M. Zhang, T. Jiang, Y. Xie, Z. Sun, and W. Li, "Additive friction stir deposition of an Al-Cu-Mg alloy: Microstructure evolution and mechanical properties," *Materials Characterization*, vol. 218, p. 114562, 2024.

[45] X. Zhu, R. Wang, L. Wang, M. Liu, and S. Li, "Effect of rotational shear and heat input on the microstructure and mechanical properties of large-diameter 6061 aluminium alloy additive friction stir deposition," *Crystals (Basel)*, vol. 14, no. 7, p. 581, 2024.

[46] N. I. Palya, K. Fraser, N. Zhu, J.B. Hoarston, K. Doherty, P.G. Allison, et al., "Microstructure prediction from smooth particle hydrodynamics process simulations of additive friction stir deposition," *Metallurgical and Materials Transactions A*, vol. 55A, no. 9, pp. 3601–3616, 2024.

[47] R. P. Kinser, N. Zhu, M.B. Williams, T.W. Rushing, K.J. Doherty, P.G. Allison, et al., "Effects on microstructure and mechanical properties of aluminum alloy 6061 processed via underwater additive friction stir deposition," *Journal of Manufacturing Processes*, vol. 134, pp. 932–942, 2025.

[48] M. Zhang, X. Ye, Y. Li, H. Wang, R. Lai, and Y. Li, "Effect of heat treatment states of feedstock on the microstructure and mechanical properties of AA2219 layers deposited by additive friction stir deposition," *Materials*, vol. 16, no. 24, p. 7591, 2023.

[49] Z. Y. Ma, S. R. Sharma, and R. S. Mishra, "Effect of friction stir processing on the microstructure of cast A356 aluminum," *Materials Science and Engineering: A*, vol. 433, no. 1–2, pp. 269–278, 2006.

[50] M. M. Z. Ahmed, S. Ataya, M. M. El-Sayed Seleman, A. M. A. Mahdy, N. A. Alsaleh, and E. Ahmed, "Heat input and mechanical properties investigation of friction stir welded AA5083/AA5754 and AA5083/AA7020," *Metals (Basel)*, no. 11, p. 68, 2021.

[51] M. M. Z. Ahmed, S. Ataya, M. M. E. S. Seleman, T. Allam, N. A. Alsaleh, and E. Ahmed, "Grain structure, crystallographic texture, and hardening behavior of dissimilar friction stir welded AA5083-O and AA5754-H14," *Metals (Basel)*, vol. 11, no. 2, pp. 1–16, 2021.

[52] M. M. Jalilvand, Y. Mazaheri, A. Heidarpour, and M. Roknian, "Development of A356/Al2O3 + SiO2 surface hybrid nanocomposite by friction stir processing," *Surface and Coatings Technology*, vol. 360, pp. 121–132, 2019.

[53] M. Zhang, T. Jiang, Y. Su, Z. Sun, Y. Xu, and W. Li, "Study on the interfacial bonding behavior of dissimilar aluminum alloys via additive friction stir deposition," *Progress in Natural Science: Materials International*, vol. 35, no. 2, pp. 433–439, 2025.

[54] M. Dong, Y. Li, T. Chen, C. Du, and X. Ren, "Solid-state additive manufacturing of dissimilar 7075–2024 aluminum alloys by additive friction stir deposition: Interfacial bonding and process optimization," *Journal of Materials Processing Technology*, vol. 343, p. 118989, 2025.

[55] L. Karthick, M. Mruthunjaya, S. Srinivas, R. Prasanna Venkatesh, N.K. Gurajala, M. Mothilal, et al., "Influence of tool pin profiles on aluminium alloy A356 and ceramic-based nanocomposites for light-weight structures by friction stir processing," *Advances in Materials Science and Engineering*, vol. 2024, p. 2494900, 2024.